J Mater Sci (2023) 58:157–169

Ceramics

Temperature-dependent mechanical properties of TaC and HfC

Hailiang Liu[1], Ke Tong[1], Xing Feng[1], Sha Liu[1], and Bin Wen[1,*]

[1] State Key Laboratory of Metastable Materials Science and Technology, Yanshan University, Qinhuangdao 066004, China

Received: 3 September 2022
Accepted: 27 November 2022
Published online: 12 December 2022

ABSTRACT

TaC and HfC are recognized as potential ultra-high temperature ceramics for application in refractories and coating materials. However, the test of mechanical property under high temperature is difficult. In this paper, the mechanical properties of TaC and HfC at high temperature are systematically investigated by density functional theory. The results revealed that their elastic constants, elastic moduli and elastic anisotropy all display a monotonic decreasing trend with increasing temperature, and the anisotropy of TaC is stronger than that of HfC at a given temperature. TaC and HfC both have eight possible dislocations. As the applied shear stress increases, the activation energies and critical resolved shear stress (CRSS) of all dislocations are decreased. As the temperature increases, the CRSS is decreased. Moreover, the yield strength and hardness of TaC and HfC both decreased with the increase of temperature. The hardness decrease from 0 to 400 K is mainly due to the proportion change of the two major dislocations ($1/2\langle 1\bar{1}0\rangle$ 0° perfect dislocations and $1/6\langle 1\bar{2}1\rangle$ 30° partial dislocations). Then the hardness sharply decreases at 400 K, which is attributed to the activation of $1/6\langle 11\bar{2}\rangle$ 90° partial dislocations. The hardness decrease from 500 K is attributed to the CRSS change of $1/6\langle 11\bar{2}\rangle$ 90° partial dislocations and $1/6\langle 1\bar{2}1\rangle$ 30° partial dislocations. In addition, the influence of strain rate and dislocation density are revealed, which shows that their hardness are both increased with increasing strain rate, while decreased with increasing dislocation density.

Introduction

Ultra-high temperature ceramics (UHTCs) have been attracting considerable attention due to their outstanding properties such as high melting point, fine chemical and thermal stability, excellent wear resistance, as well as high strength and hardness [1–3]. Transition metal carbides (TMCs) belong to a typical subset of UHTCs, among which TaC and HfC are outstanding for their extremely high melting point (near 4000 °C) [4], making them potential materials

Handling Editor: David Cann.

Address correspondence to E-mail: wenbin@ysu.edu.cn

https://doi.org/10.1007/s10853-022-08026-6

applied in the field of refractories and coating materials [5]. Besides, these B1-structure refractory carbides or nitrides are a significant strengthening phase in the design of refractory alloys [6, 7]. Therefore, their mechanical properties under high temperature need to be explored for structural design in practical application.

A number of experimental research on TaC and HfC have been made in the past years. Ferro et al. [8] evaluated the hardness of HfC using an area law-of-mixtures approach with respect to the indentation size effect. Zhang et al. [9] revealed that high temperature densification can enhance the mechanical properties of TaC. However, due to the complexity of sample preparation and the difficulty of experimental process, very few studies have been performed on the mechanical properties at high temperature. Nowadays, with the development of first-principles calculation based on density functional theory (DFT), it is possible to accurately predict the mechanical properties at high temperature. Sai Gautam et al. [10] investigated the mechanical properties and thermochemical properties of TaC and HfC with respect to pressure via first principles calculations. Yu et al. [11] studied the stability of various tantalum carbides at 0 K by first-principles simulations, and they also clarified the relationship between phase content and mechanical properties. Throughout these publications, although some achievements have been made in the past, the influence of temperature on mechanical properties has not been involved in their methods, and the plastic deformation mechanisms of TaC and HfC under high temperature are not well-known, which restricts the further development of TaC and HfC. In our method, the mechanical properties at high temperature is innovatively determined by first principles calculation and quasi-harmonic approximation (QHA).

In this paper, the temperature-dependent mechanical properties of TaC and HfC were investigated based on the theoretical methods proposed by Wen et al. [12] and Feng et al. [13]. Firstly, the stability of the two TMCs was verified. Their elastic constants, elastic moduli and elastic anisotropy were calculated and analyzed. The possible dislocations were determined and the activation energy and CRSS of each dislocation were calculated. Furthermore, the yield strength and hardness of the two TMCs were calculated, and the deformation mechanism at high temperature were revealed. In addition, the influence of strain rate and dislocation density on hardness was also discussed.

Computational methods

DFT calculations

The DFT calculations in this work were performed by the Vienna ab-initio Simulation Package (VASP) [14]. The generalized gradient approximation (GGA) with the Perdew-Burke-Ernzerhoff (PBE) [15, 16] exchange correlation functions was applied to evaluate the exchange–correlation energy. The interaction between ions and electrons was described by projector augmented wave (PAW) potential [17]. The cut-off energy of plane-wave used was 600 eV. The energy threshold was set as 10^{-5} eV/atom and the force threshold of ionic relaxation was set to be 0.01 eV/Å. The Debye frequency is defined as the maximal value of phonon frequencies, which can be determined by the finite displacement method using PHONOPY code [18]. The Debye frequencies of TaC and HfC have been determined to be 18.23 THz and 17.12 THz, respectively.

Temperature-dependent elastic constants

Based on the "geometry optimization method for arbitrary symmetry crystals" (GOMASC) method proposed by Wen et al. [12, 19], the Helmholtz free energy $F[X(\varepsilon);T]$ can be expressed as follow [19]:

$$F[X(\varepsilon);T] = E[X(\varepsilon)] + F_{vib}[X(\varepsilon);T] \quad (1)$$

where $X(\varepsilon)$ is the crystal lattice with a strain of ε, $E[X(\varepsilon)]$ represents the static energy of the crystal lattice $X(\varepsilon)$ at 0 K, $F_{\mathrm{vib}}[X(\varepsilon);T]$ is the vibrational Helmholtz free energy obtained based on quasi-harmonic assumption. Isothermal constants $C_{ij}(T)$ can be obtained from the derivative of $F[X(\varepsilon);T]$. There are three independent constants (C_{11}, C_{12} and C_{44}) for a cubic crystal. In order to construct linear equations to acquire elastic constants, three forms of deformation, namely [δ, δ, δ, 0, 0, 0], [δ, -δ, $\delta^2/(1\text{-}\delta^2)$, 0, 0, 0] and [$\delta^2/(1\text{-}\delta^2)$, 0, 0, 2$\delta$, 0, 0] are needed.

According to Ref. [20] and [21], the Young's modulus (E), bulk modulus (B), and shear modulus (G) can be expressed as follow:

$$B_V = B_R = (C_{11} + C_{12})/3 \quad (2)$$

$$G_V = (C_{11} - C_{12} + 3C_{44})/5 \quad (3)$$

$$G_R = 5(C_{11} - C_{12})C_{44}/[4C_{44} + 3(C_{11} - C_{12})] \quad (4)$$

$$B = (B_V + B_R)/2 \quad (5)$$

$$G = (G_V + G_R)/2 \quad (6)$$

$$E = 9BG/(3B + G) \quad (7)$$

where V and R subscripts are Voigt and Reuss estimates, respectively.

Generalized stacking fault energy

The plastic deformation of crystalline materials is usually correlated to the slip of dislocations. Generalized stacking fault energy (GSFE) distributions are utilized to identify the possible types of dislocations. The GSFE was calculated via slab model. For each kind of slip plane, a supercell structure with 16 atoms was built, with the slip plane located in the middle. A vacuum layer with a thickness of 15 Å was set on the side of supercell parallel to the slip plane. The atom above the slip plane were rigidly moved with a Burgers vector $\boldsymbol{b}$. Then the slipped supercell was relaxed in the direction perpendicular to the slip plane. The GSFE is the increased energy compared to the un-slipped supercell. The Brillouin zone in k-space was sampled by Monkhorst–Pack mesh [22] of 7 × 7 × 1. The energy convergence threshold was set to be 1×10^{-5} eV/atom.

Temperature-dependent yield strength

According to Feng's method [13], the activation energy $W_c(\tau)$ of dislocation can be considered as a function of applied stress τ as follow:

$$W_c(\tau) = \frac{A_1 G b^2 h}{2\pi} \ln\left(\frac{x_c}{r}\right) - (hb)^{3/2}\left(\frac{A_2 G \tau}{2\pi}\right)^{1/2} \quad (8)$$

$$A_1 = \cos^2\beta + \frac{\sin^2\beta}{1-v} \quad (9)$$

$$A_2 = \frac{(1+v)\cos^2\beta + (1-2v)\sin^2\beta}{1-v} \quad (10)$$

where x_c is the critical width of kink pair, b is the Burgers vector, h is the kink height, G is the shear modules, r represents the radius of dislocation core, β is the angle between the dislocation line and Burgers vector, v is Poisson's ratio.

The temperature-dependent critical resolved shear stress (CRSS) at a given temperature T, applied stress τ, and plastic strain rate $\dot{\varepsilon}$ can be expressed as:

$$\tau_{\mathrm{CRSS}}^{T} = \frac{2\pi}{A_2 h^3 b^3 G}\left[\frac{A_1 G b^2 h}{2\pi}\ln\left(\frac{x_c}{r}\right) - k_B T ln\left(\frac{\rho_m b \lambda_b v_D}{\dot{\varepsilon}}\right)\right] \quad (11)$$

where v_D and ρ_m are the Debye frequency and density of mobile dislocations, respectively. λ_b indicates the mean free path for dislocations crossing the barrier, k_B represents the Boltzmann constant.

Based on the calculated CRSS of dislocation, the temperature-dependent yield strength of polycrystalline are calculated according to Sachs model [23]. A polycrystalline model with 30,000 randomly oriented gains was built. When the proportion of plastically yielded grains reaches 90% [24], the corresponding uniaxial stress is defined as the yield stress of polycrystalline. According to Tabor's law, the hardness is approximately three times of the yield stress [25], based on which, the temperature-dependent hardness of TaC and HfC were calculated.

Results and discussion

Stability

TaC and HfC are both NaCl-type structure, as shown in Fig. 1. The relaxed lattice parameters of TaC (4.47 Å) and HfC (4.65 Å) are in good agreement with experimental values [26, 27]. The phonon spectrum of TaC and HfC at various temperatures are calculated and illustrated in Fig. 2. It is seen that the phonon spectrum of TaC (Fig. 2a) and HfC (Fig. 2b) do not

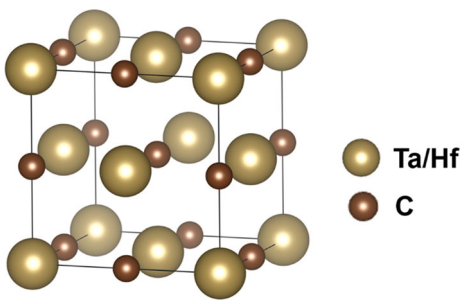

Figure 1 Crystal structure of TaC and HfC.

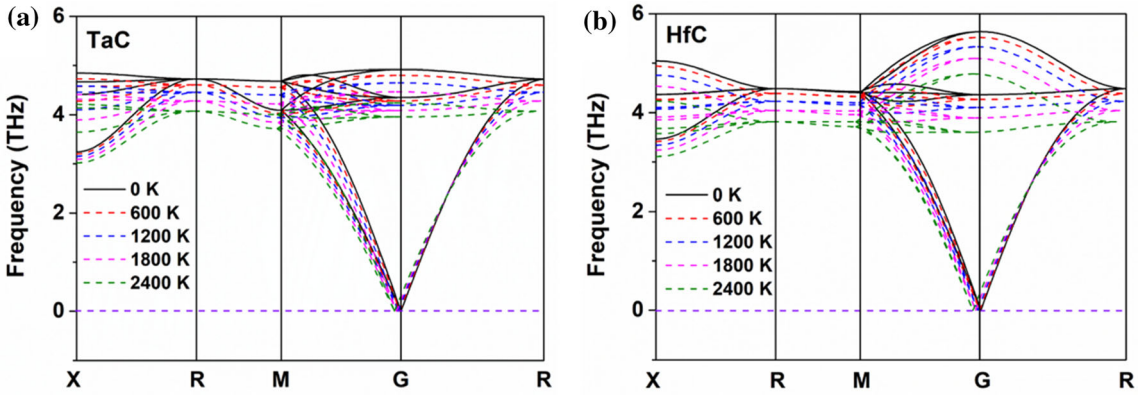

Figure 2 Phonon spectrum of **a** TaC and **b** HfC at different temperature.

have any imaginary frequencies, which indicates that TaC and HfC are both dynamically stable [28, 29]. It should be noted that the phonon frequencies of the two TMCs both decrease with the increasing temperature. This phenomenon is because that with increasing temperature, the atomic distance is generally increased, which results in a smaller force constant and a lower phonon frequency.

Temperature-dependent elastic properties

The temperature-dependent elastic constants and elastic modulus of TaC and HfC were obtained, and the results are shown in Fig. 3. It is seen that the elastic constants and modulus both show a monotonic decreasing trend with temperature rising, and the values of elastic constants and elastic modulus of TaC are both higher than those of HfC at a given temperature, indicating that TaC possesses relatively more excellent elastic properties than HfC. Our results are compared with other research in Table 1. As can be seen, there exists a good consistency between our calculated results and other available researches for TaC [30–32] and HfC [30, 33, 34].

In order to efficiently investigate and visualize the anisotropic elastic properties of TaC and HfC, the 3D surfaces of Young's modulus E and shear modulus G at different temperatures for the two TMCs were plotted by using ELAM code [35], as shown in Fig. 4. From Fig. 4a and b, the maximal value of the Young's modulus for the two TMCs both appear in $< 100 >$ direction, and the minimal value both locate in $< 111 >$ direction. The 3D surface of the shear modulus (Fig. 4c and d) contains two kinds of surfaces, in which the solid one inside denotes the minimal values, while the translucent one outside denotes the maximal values. Figure 5a–d shows the 2D projections of the 3D surface on {100} plane, where different temperatures are denoted by different colors, and the maximum and minimum values are denoted by solid and dash curves, respectively. It is seen that Young's modulus and shear modulus for the two TMCs are both decreased with increasing temperature, and the maximum and minimum value of shear modulus are both in the $< 110 >$ direction. In addition, it should be noted that the maximum and minimum value of shear modulus for HfC nearly overlapped at 1200 K (Fig. 4d), which indicates that the gap between the maximum value and the minimum value is getting smaller and nearly closed to zero with the increase of temperature. The decreasing speed of the maximum value is higher than that of the minimum value.

The extent of the 3D surface deviated from sphere can reflect the extent of anisotropy [36]. It is noted that the 3D surfaces of Young's modulus and shear modulus for the two TMCs (Fig. 4) both tend to be spherical with increasing temperature, which means their anisotropy are both weaken. This can also be reflected by the shape of the projection in Fig. 5, where the 2D projection tend to be circular with the increase of temperature. At a given temperature, the 3D surface of HfC is always closer to spherical, which means its elastic anisotropy is relatively weaker. To quantify the elastic anisotropy of TaC and HfC, the anisotropy index A^U is expressed as follows [37]:

$$A^U = 5\frac{G_V}{G_R} + \frac{B_V}{B_R} - 6 \geq 0 \tag{12}$$

For an isotropic crystal, A^U is identically zero. A large value of A^U means the elastic anisotropy is strong. The elastic anisotropy index of the two TMCs

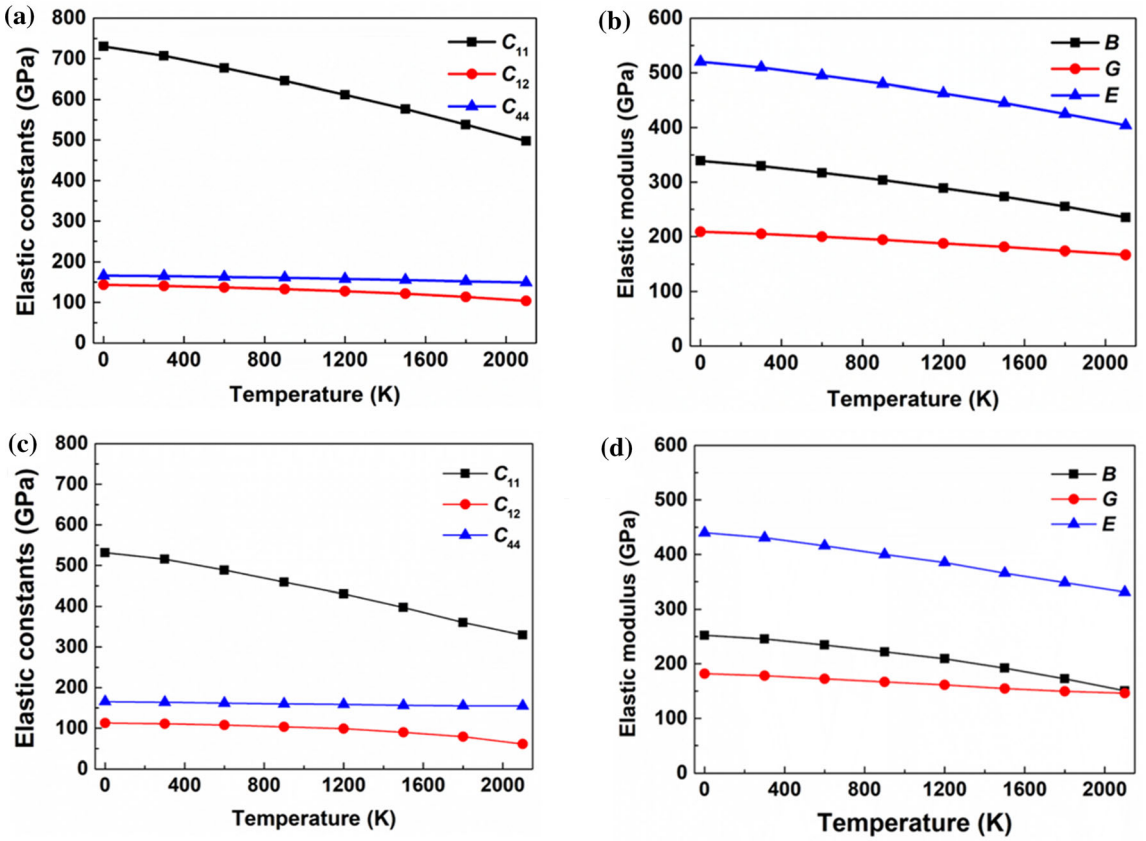

Figure 3 Temperature-dependent elastic properties of TaC and HfC. **a** Elastic constants of TaC. **b** Elastic modulus of TaC. **c** Elastic constants of HfC. **d** Elastic modulus of HfC.

Table 1 Comparison of our calculated elastic constants C_{ij}, bulk modulus B, shear modulus G, Young's modulus E with other research

Carbides	Method	Elastic constants			Elastic modulus			
		C_{11}	C_{12}	C_{44}	B	G	E	v
TaC	Present	730.2	143.4	166.1	339.0	209.0	520.1	0.24
	Calc. [32]	708	132	176	324	215		0.23
	Expt. [30]				344	216	537	0.24
	Calc [31]				317	209	514	0.23
HfC	Present	531.5	112.8	165.4	252.3	181.7	439.7	0.21
	Calc. [34]	527.1	107.1	160.0	247.1	178.4	431.4	0.21
	Expt. [33]	500		180				
	Expt. [30]				242	195	461	0.18

at different temperatures were calculated, as shown in Fig. 5e. The elastic anisotropy index for the two TMCs both descend with temperature, indicating a weaken tendency. Meanwhile, the anisotropic index of HfC is always smaller than that of TaC at any given temperature, indicating a relatively stronger anisotropy of TaC.

Dislocations slip mechanism

It is reported that the favorable slip system in TaC is < 110 > {111} [38, 39], whereas in HfC is < 110 > {110} [40], where they are both low-indexed planes and directions. In order to comprehensively explore the deformation mechanism of TaC and HfC, three low index planes {111}, {110} and {100} were selected to determine the dislocation types. The calculated

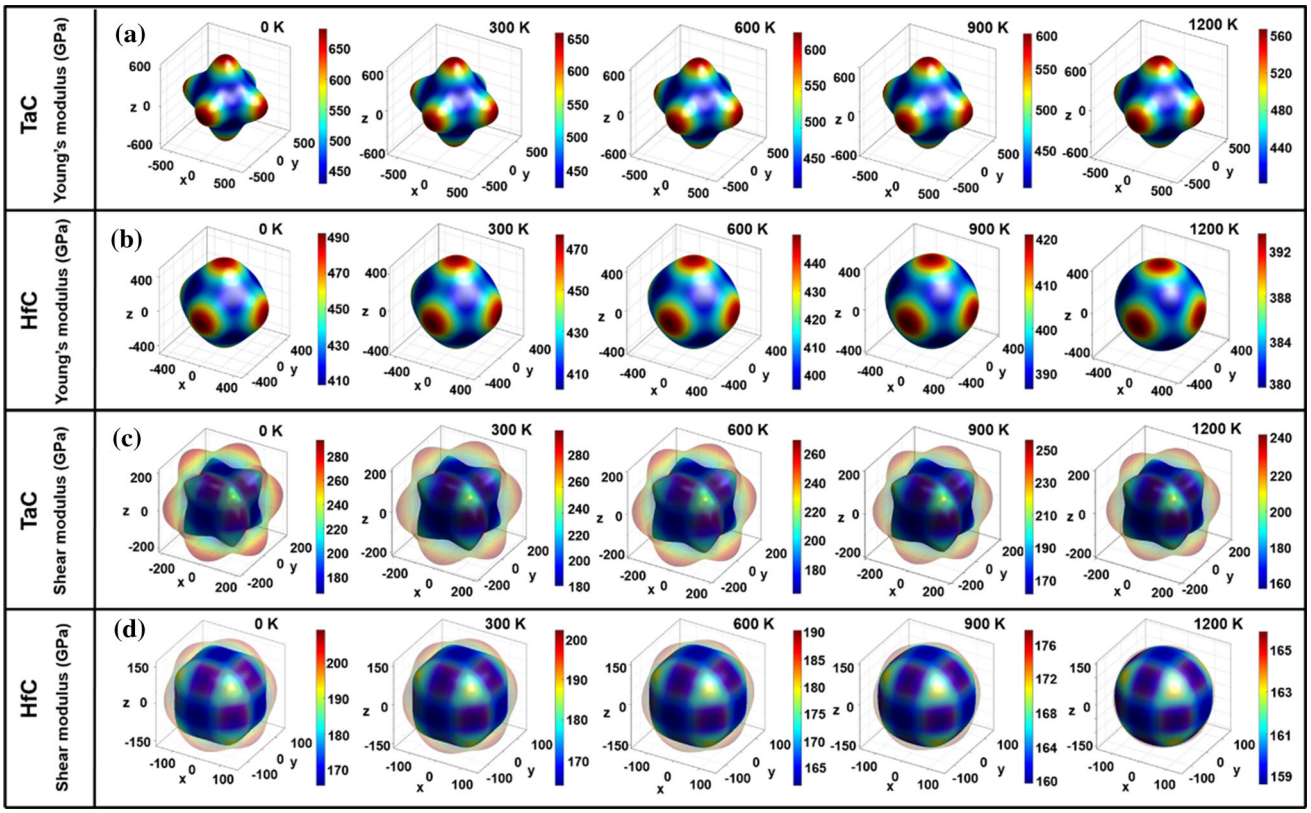

Figure 4 Temperature-dependent 3D surface of Young's modulus and shear modulus for TaC and HfC. **a** Young's modulus for TaC. **b** Young's modulus for HfC. **c** Shear modulus for TaC. **d** Shear modulus for HfC. The unit is GPa.

GSFE distributions are displayed in Fig. 6. Local minima of GSFE distribution corresponds to the stable stacking fault which leads to the dissociation of dislocations. From Fig. 6, the GSFE distribution of the two TMCs are very similar, which is attributed to their same crystal structure. On {111} plane (Fig. 6a and b), there are three kinds of possible perfect dislocations, namely $1/2[1\bar{1}0]$ 0° perfect dislocation, $1/2[10\bar{1}]$ 60° perfect dislocation and $1/2[01\bar{1}]$ 60° perfect dislocation. There is a local energy minimum along $[1\bar{2}1]$ direction with 1.78 J/m^2 for TaC and 3.38 J/m^2 for HfC, respectively, which leads to the decomposition of the perfect dislocations. According to the geometric and energy conditions of dislocation dissociation, the perfect dislocation on {111} plane can be dissociated as:

$$1/2[1\bar{1}0] \rightarrow 1/6[1\bar{2}1] + 1/6[2\bar{1}1] \quad (13)$$

$$1/2[01\bar{1}] \rightarrow 1/6[\bar{1}2\bar{1}] + 1/6[11\bar{2}] \quad (14)$$

$$1/2[10\bar{1}] \rightarrow 1/6[11\bar{2}] + 1/6[2\bar{1}1] \quad (15)$$

Thus, there may be four kinds of dislocations on {111} plane for TaC and HfC: $1/2[1\bar{1}0]$ 0° perfect dislocations, $1/2[01\bar{1}]$ 60° perfect dislocations, $1/6[1\bar{2}1]$ 30° partial dislocations and $1/6[11\bar{2}]$ 90° partial dislocations. From Fig. 6c and d, there are two kinds of perfect dislocations on {110} plane. There is no local energy minimum on this plane, which means the perfect dislocations on {110} plane would not be dissociated. Therefore, there are only two types of dislocations on the TaC and HfC on this plane: $1/2[1\bar{1}0]$ 0° perfect dislocation and [001] 90° perfect dislocations. From Fig. 6e and f, there are two kinds of perfect dislocations $1/2[01\bar{1}]$ 0° and 1/2[011] 90° perfect dislocations on {100} plane. There is no local energy minimum on this plane, suggesting that the two perfect dislocations will not be decomposed. Therefore, there are only these two types of perfect dislocations on {100} plane. Based on the GSFE distributions, all possible dislocations of the two TMCs are listed in Table 2.

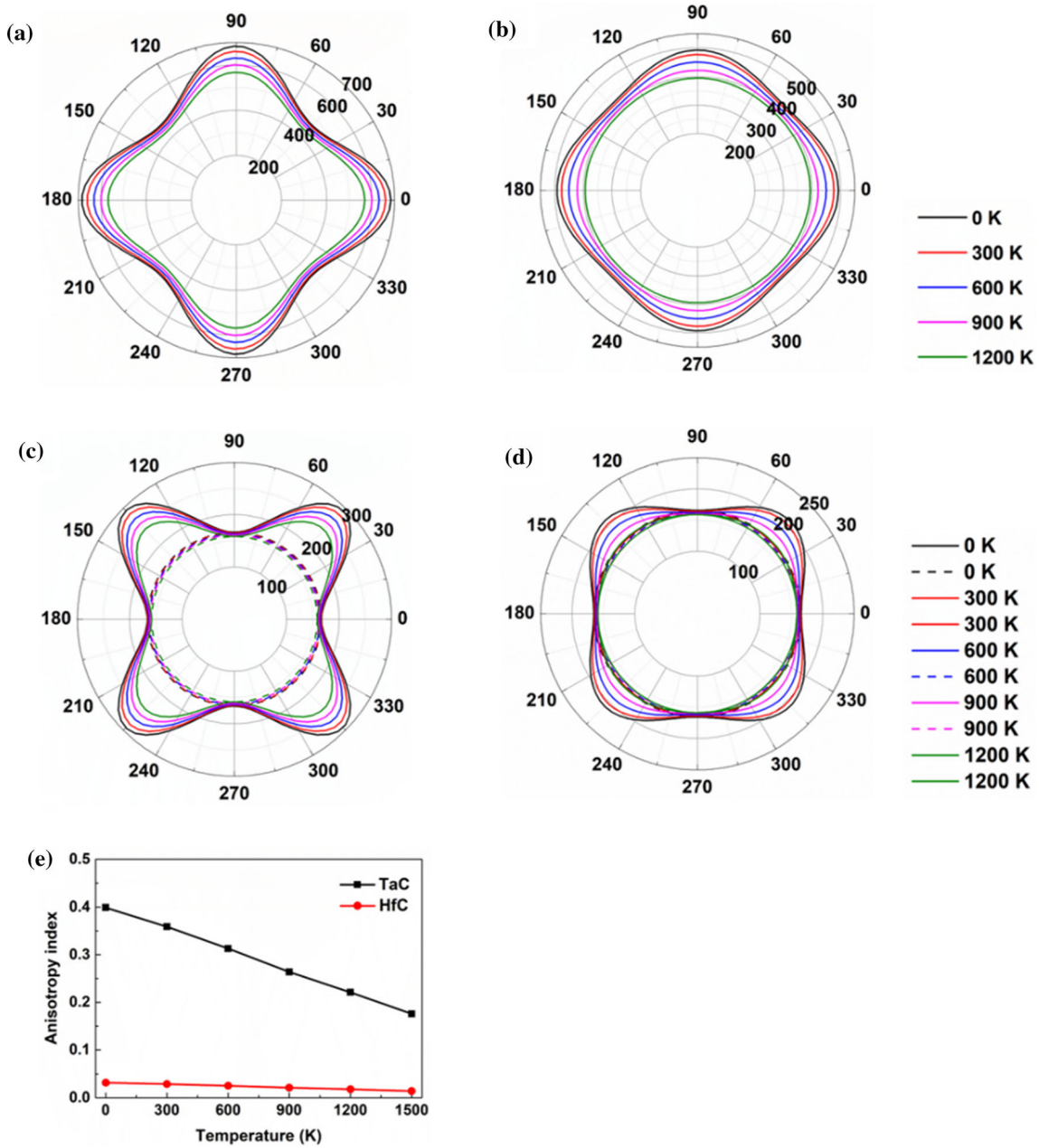

Figure 5 Projections of elastic moduli on {100} plane and anisotropy index at different temperatures. **a** Young's modulus of TaC. **b** Young's modulus of HfC. **c** Shear modulus of TaC. **d** Shear modulus of HfC. **e** Anisotropy index for TaC and HfC.

Temperature-dependent strength/hardness

The activation energies of all dislocations in TaC and HfC as a function of applied stress are shown in Fig. 7. It is seen that the activation energies of all dislocations are decreasing with increasing applied stress. The activation energies of dislocations on {111} and {100} planes intersect with each other, indicating that there exists a competitive relationship between different dislocations. Based on the activation energy, the CRSSs of all dislocations as a function of temperature were calculated and shown in Fig. 8. It is seen that the CRSS of all dislocations decrease monotonically as the temperature rises.

The proportion of yielded grains in polycrystalline is shown in Fig. 9a. At 0 K, the grains in TaC and HfC start to be yielded under applied stress of 5.79 GPa and 4.96 GPa respectively, and 90% grains are yielded under applied stress of 7.95 GPa and 7.10 GPa,

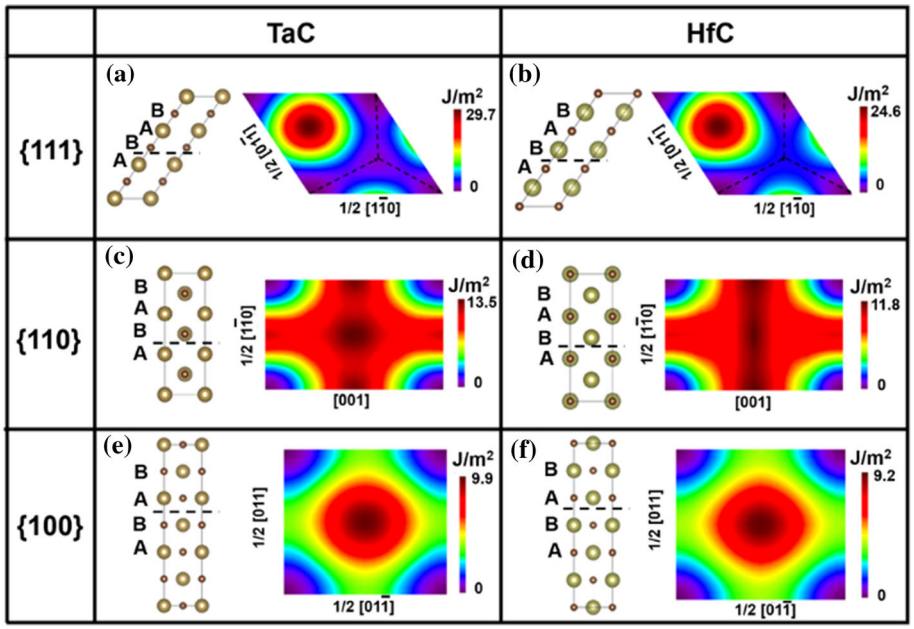

Figure 6 GSFE distributions of TaC and HfC on {111}, {110}, and {100} planes.

Table 2 Dislocation types on slip planes of TaC and HfC

Slip plane	Dislocation type	b (Å)		h (Å)	
		TaC	HfC	TaC	HfC
{111}	$1/6\langle 11\bar{2}\rangle$ 90° partial dislocations	1.827	1.896	2.740	2.845
	$1/6\langle 1\bar{2}1\rangle$ 30° partial dislocations	1.827	1.896	2.740	2.845
	$1/2\langle 1\bar{1}0\rangle$ 0° perfect dislocations	3.164	3.285	2.740	2.845
	$1/2\langle 01\bar{1}\rangle$ 60° perfect dislocations	3.164	3.285	2.740	2.845
{110}	$1/2\langle 1\bar{1}0\rangle$ 0° perfect dislocations	3.164	3.285	4.475	4.646
	$\langle 001\rangle$ 90° perfect dislocations	4.475	4.646	4.475	4.646
{100}	$1/2\langle 011\rangle$ 90° perfect dislocations	3.164	3.285	3.164	3.285
	$1/2\langle 01\bar{1}\rangle$ 0° perfect dislocations	3.164	3.285	3.164	3.285

respectively. When the temperature reaches 300 K, the grains in TaC and HfC start to be yielded under applied stress of 3.81 GPa and 3.21 GPa respectively, and 90% grains are yielded under applied stress of 6.85 GPa and 6.08 GPa respectively. It can be concluded that the yield strength of the two TMC polycrystalline are both decreased with the increase of temperature.

The temperature-dependent hardness of TaC and HfC are shown in Fig. 9b. It is seen that the hardness of TaC and HfC are both decreased with increasing temperature. The hardness of the two TMCs at room temperature (300 K) are 20.57 GPa for TaC and 18.25 GPa for HfC, which is in good agreement with experimental values [8, 9, 41–44]. In order to better understand the mechanism of plastic deformation at high temperature, the proportion of grains yielded by different dislocations were calculated, and the results are shown in Fig. 10. The two TMCs possess almost the same dislocation proportions at any given temperature. From 0 to 400 K, the plastic deformation of TaC and HfC are both governed by $1/2\langle 1\bar{1}0\rangle$ 0° perfect dislocations, $1/6\langle 1\bar{2}1\rangle$ 30° partial dislocations, $1/2\langle 01\bar{1}\rangle$ 0° perfect dislocations and $1/2\langle 011\rangle$ 90° perfect dislocations, with the former two being the majority. In this temperature range, the proportion of $1/2\langle 1\bar{1}0\rangle$ 0° perfect dislocations decreases, while that of $1/6\langle 1\bar{2}1\rangle$ 30° partial dislocations increases (the other two dislocations are minorly changed) as the temperature rises. The CRSS of $1/2\langle 1\bar{1}0\rangle$ 0° perfect dislocation decreases slightly as the temperature rises, while that of $1/6\langle 1\bar{2}1\rangle$ 30° partial dislocations drop dramatically (Fig. 8), so the decrease in

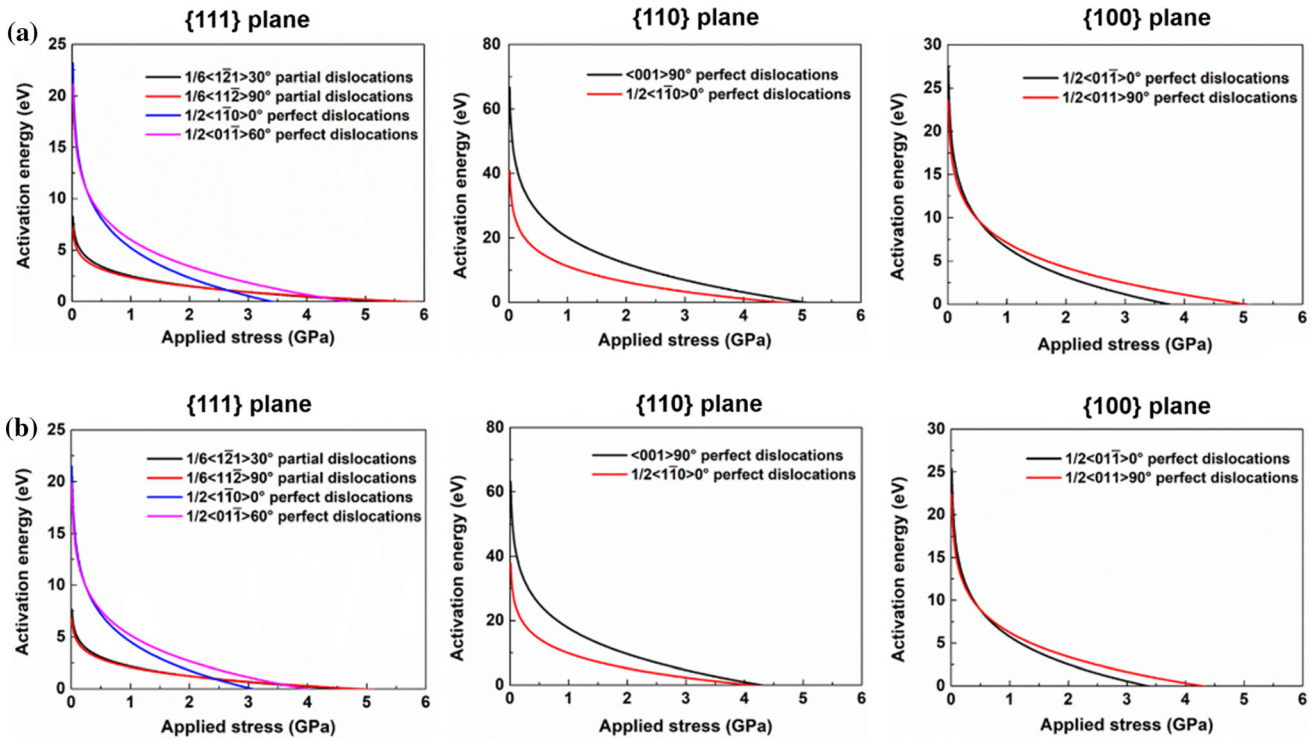

Figure 7 Activation energy of dislocations on {111}, {100} and {110} planes as a function of applied stress. **a** TaC; **b** HfC.

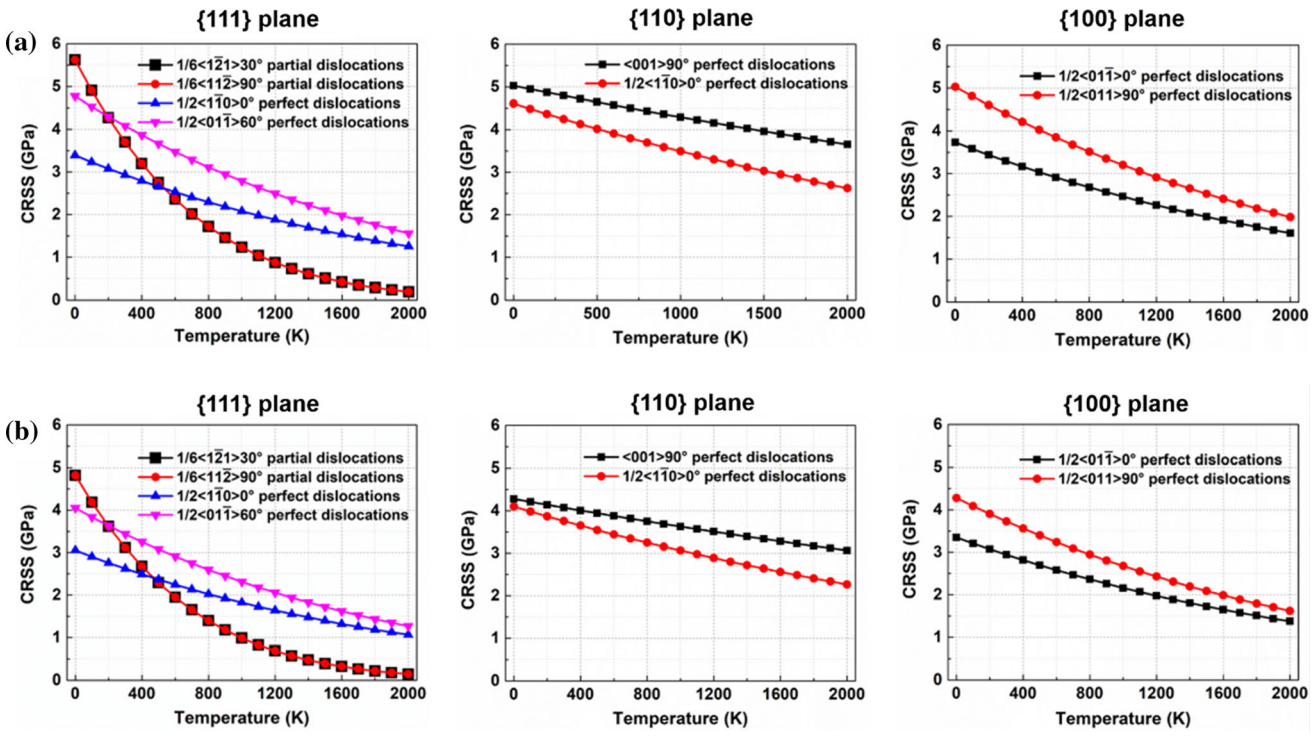

Figure 8 Temperature-dependent CRSS of dislocations on {111}, {110} and {100} planes. **a** TaC; **b** HfC.

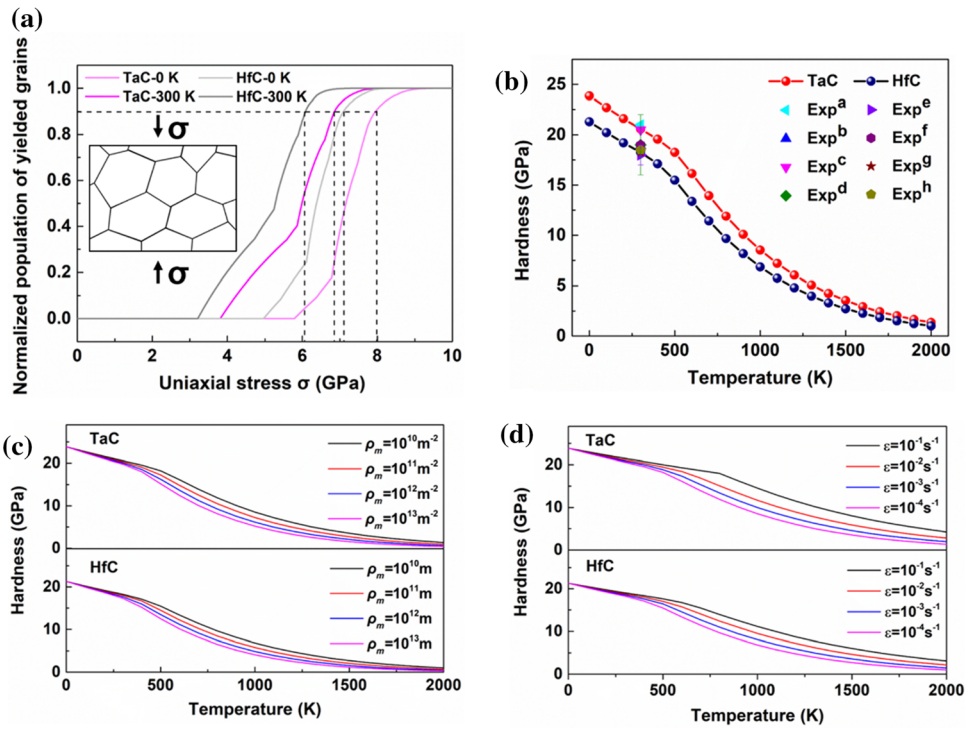

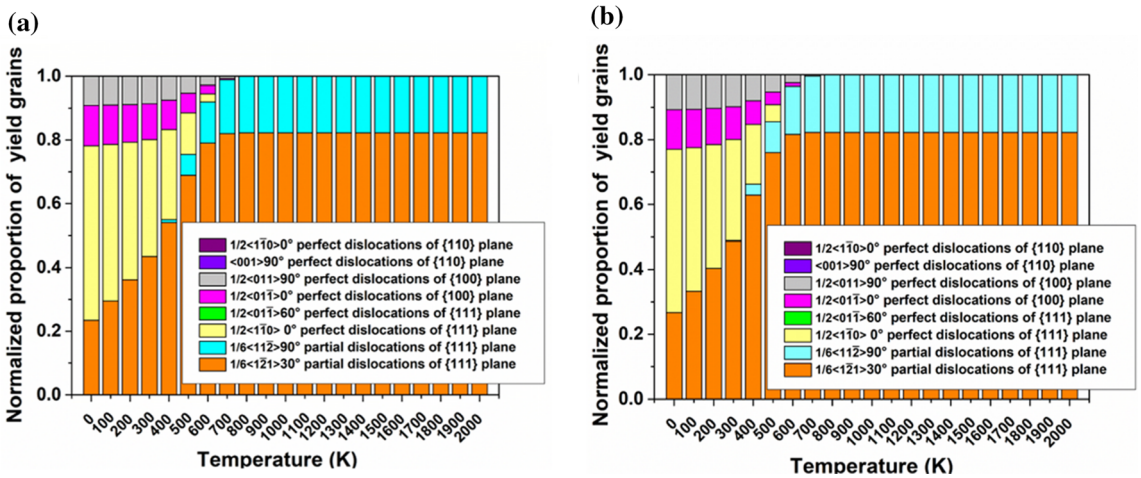

Figure 9 **a** Proportion of yielded grains as a function of uniaxial stress. **b** Comparison between our calculated hardness with experiments ([a]Ref. [9], [b]Ref. [41], [c]Ref. [42], [d]Ref. [43], [e]Ref. [43], [f]Ref. [8], [g]Ref. [41], [h]Ref. [44]). **c** Temperature-dependent hardness under various dislocation density. **d** Temperature-dependent hardness under various strain rates.

Figure 10 Proportion of activated dislocations at different temperature. **a** TaC; **b** HfC.

hardness from 0 to 400 K (Fig. 9(b)) can be attributed to the proportion change as well as the sharply decreased CRSS of $1/6\langle 1\bar{2}1\rangle$ 30° partial dislocations. Above 400 K, depart from the four dislocations, $1/6\langle 11\bar{2}\rangle$ 90° partial dislocations are also activated, whose CRSS is the same as the $1/6\langle 1\bar{2}1\rangle$ 30° partial dislocations (Fig. 8), so the sudden drop in hardness at 400 K (Fig. 9b) is due to the total proportion of $1/6\langle 11\bar{2}\rangle$ 90° partial dislocations and $1/6\langle 1\bar{2}1\rangle$ 30° partial dislocations reaches a very large value. As temperature rises, their total proportion continually increases, which exceeds 70% at 500 K and reaches 100% at 800 K.

In addition, the influence of dislocation density and strain rates on hardness were also studied, and the results are shown in Fig. 9c and d. It is found that under a given temperature, as the dislocation density rises, the hardness of TaC and HfC are both decreased. As the strain rate rises, the hardness of TaC and HfC are both increased. This means that the dislocation density and strain rate have great influence on the hardness of materials.

Conclusions

In this paper, the mechanical properties of TaC and HfC at high temperature were explored via first-principles calculations, and the main conclusions were obtained as following:

(1) TaC and HfC are both dynamically stable, and their phonon frequencies are decreased as the temperature rises.
(2) The elastic constants, elastic moduli and elastic anisotropy of TaC and HfC all show a monotonic decreasing tendency as temperature rises. At a given temperature, the anisotropy of TaC is stronger than that of HfC.
(3) TaC and HfC both have eight possible dislocation types by analyzing the GSFE surfaces. The activation energies of all dislocations are decreased with applied shear stress. The CRSS of all dislocations is decreased with temperature.
(4) The yield strength and hardness of TaC and HfC are both decreased as temperature rises. The decrease in hardness from 0 to 400 K is attributed to the increased proportion as well as the sharply decreased CRSS of $1/6\langle 1\bar{2}1\rangle$ 30° partial dislocations. The sudden drop in hardness at 400 K is attributed to the total proportion of $1/6\langle 11\bar{2}\rangle$ 90° partial dislocations and $1/6\langle 1\bar{2}1\rangle$ 30° partial dislocations reaches a very large value. The hardness decrease above 500 K is mainly attributed to the continually increased proportion as well as the continually decreased CRSS of $1/6\langle 1\bar{2}1\rangle$ 30° partial dislocations and $1/6\langle 11\bar{2}\rangle$ 90° partial dislocations.
(5) Under a given temperature, as the dislocation density rises, the hardness of TaC and HfC is both decreased. As the strain rate rises, the hardness of TaC and HfC is both increased.

Acknowledgements

This work was supported by the National Natural Science Foundation of China (Grant Nos. 51925105, 51771165), National Key R&D Program of China (Grant No. YS2018YFA070119) and National Postdoctoral Program for Innovative Talents (Grant No. BX20200285).

Declarations

Conflict of interest The authors declare that they have no conflict of interest.

References

[1] Jhi SH, Louie SG, Cohen ML, Ihm J (2001) Vacancy Hardening and Softening in Transition Metal Carbides and Nitrides. Phys Rev Lett 86(15):3348
[2] Csanádi T, Castle E, Reece M, Dusza J (2019) Strength enhancement and slip behaviour of high-entropy carbide grains during micro-compression. Sci Rep 9:10200
[3] Toth Louis E (1971) Transition Metal Carbides and Nitrides. Academic Press, New York and London
[4] Hong QJ, Walle AVD (2015) Prediction of the material with highest known melting point from Ab initio molecular dynamics calculations. Phys Rev B 92(2):020104
[5] Cedillos-Barraza O, Grasso S, Nasiri NA, Jayaseelan D, Reece MJ, Lee WE (2016) Sintering behaviour, solid solution formation and characterisation of Tac, Hfc and Tac-Hfc fabricated by spark plasma sintering. J Eur Ceram Soc 36(7):1539
[6] Xg A, Liang WB, Ng A, Ll B, Gz A, Cs A, Ys B, Jg B (2021) Microstructure and mechanical properties of multi-phase reinforced Hf-Mo-Nb-Ti-Zr refractory high-entropy alloys. Inter J Refract Metals Hard Mater 102:105723
[7] Yang C, Bian H, Aoyagi K, Hayasaka Y, Yamanaka K, Chiba A (2021) Synergetic strengthening in hfmonbtati refractory high-entropy alloy via disordered nanoscale phase and semicoherent refractory particle. Mater Des 212:110248
[8] Ferro D, Barinov SM, Rau JV, Latini A, Scandurra R, Brunetti B (2006) Vickers and knoop hardness of electron beam deposited Zrc and Hfc thin films on titanium. Surf Coat Technol 200(16):4701
[9] Zhang Z, Liang H, Chen H, Wang J, Peng F, Cheng Lu (2019) Exploring physical properties of tantalum carbide at high pressure and temperature. Inorg Chem 59(3):1848–1852
[10] Gautam GS, Kumar KH (2014) Elastic, thermochemical and thermophysical properties of rock salt-type transition metal carbides and nitrides: a first principles study. J Alloy Compd 587:380
[11] Yu X, Weinberger C, Thompson G (2014) Ab initio investigations of the phase stability in tantalum carbides. Acta Mater 80:341
[12] Wen B, Shao T, Melnik R, Kawazoe Y, Tian Y (2013) Temperature and pressure dependent geometry optimization and elastic constant calculations for arbitrary symmetry

crystals: applications to Mgsio3 Perovskites. J Appl Phys 113(10):103501
[13] Feng X, Xiao J, Wen B, Zhao J, Xu B, Wang Y, Tian Y (2021) Temperature-dependent hardness of Zinc-Blende structured covalent materials. Sci. China-Mater 64(9):2280
[14] Hafner J (2008) Ab-initio simulations of materials using vasp: density-functional theory and beyond. J Comput Chem 29:2044
[15] Kresse G, Furthmüller J (1996) Efficient iterative schemes for ab initio total-energy calculations using a plane-wave basis set. Phys Rev B 54:11169
[16] Perdew JP, Burke K, Ernzerhof M (1996) Generalized gradient approximation made simple. Phys Rev Lett 77(18):3865
[17] Blöchl PE (1994) Projector augmented-wave method. Phys Rev B 50:17953
[18] Mann S, Rani P, Kumar R, Jindal VK (2015) DFT study of phonon dispersion in pure graphene. AIP Publishing.
[19] Shao T, Wen B, Melnik R, Shan Y, Kawazoe Y, Tian Y (2012) Temperature Dependent Elastic Constants for Crystals with Arbitrary Symmetry: Combined First Principles and Continuum Elasticity Theory. J Appl Phys 111(8):137
[20] Haines J, Leger JM, Bocquillon G (2001) Synthesis and design of superhard materials. Annu Rev Mater Res, Palo Alto, pp 1–23
[21] Hill R (1952) The elastic behaviour of a crystalline aggregate. Proceed Phys Soci 65(5):349
[22] Monkhorst HJ, Pack JD (1976) Special points for brillouin-zone integrations. Phys. Rev. B 13(12):5188–5192
[23] Barnett MR, Student ZK, Ma X (2006) A semianalytical sachs model for the flow stress of a magnesium alloy. Metall and Mater Trans A 37(7):2283
[24] Zong C, Mao WM, Zhu GH (2014) Analysis of yield strength anisotropy of pipeline steel based on crystallographic model. Mater ence Technol 30(12):1419
[25] Cahoon JR, Broughton WH, Kutzak AR (1971) The determination of yield strength from hardness measurements. Metall Transact 2(7):1979–1983
[26] Bowman A (1961) The variation of lattice parameter with carbon content of tantalum carbide. J Phys Chem 65:1596
[27] Villars P, Calvert LD, Pearson WB (1985) Pearson's Handbook of Crystallographic Data for Intermetallic Phases. Acta Cryst 40(a1):C444
[28] Togo A, Tanaka I (2015) First Principles Phonon Calculations in Materials Science. Scripta Mater 108:1
[29] Chong X, Hu M, Wu P, Shan Q, Jiang YH, Li ZL, Feng J (2019) Tailoring the Anisotropic Mechanical Properties of Hexagonal M7x3 (M=Fe, Cr, W, Mo; X=C, B) by Multialloying. Acta Mater 169:193
[30] Brown HL, Armstrong PE, Kempter CP (1966) Elastic Properties of Polycrystalline Sc, Re, Ru and Pt21 Ir. J Less-Common Metals 11(2):135
[31] Lu XG, Selleby M, Bo S (2007) Calculations of thermophysical properties of cubic carbides and nitrides using the debye-grüneisen model. Acta Mater 55(4):1215
[32] Jong M, Wei C, Angsten T, Jain A, Notestine R, Gamst A, Sluiter M, Ande CK, Zwaag S, Plata JJ (2015) Charting the complete elastic properties of inorganic crystalline compounds. Scientific Data 2:150009
[33] Weber W (1973) Lattice dynamics of transition-metal carbides. Phys Rev B 8(11):5082
[34] Hui L, Zhang L, Zeng Q, Kang G, Li K, Ren H, Liu S, Cheng L (2011) Structural, elastic and electronic properties of transition metal carbides Tmc (Tm=Ti, Zr, Hf and Ta) from first-principles calculations. Solid State Commun 151(8):602
[35] Marmier A, Lethbridge Z, Walton R, Smith C, Parker S, Evans K (2010) Elam: a computer program for the analysis and representation of anisotropic Elastic properties. Comput Phys Commun 181(12):2102
[36] Setyawan W, Curtarolo S (2010) High-throughput electronic band structure calculations: challenges and tools. Computat Mater ence 49(2):299
[37] Ranganathan SI, Ostoja-Starzewski M (2008) Universal Elastic Anisotropy Index. Phys Rev Lett 101(5):055504
[38] Rowcliffe D, Hollox G (1971) Plastic flow and fracture of tantalum carbide and hafnium carbide at low temperatures. J Mater Sci 6:1261
[39] Kim C, Gottstein G, Grummon D (1994) Plastic flow and dislocation structures in tantalum carbide: deformation at low and intermediate homologous temperatures. Acta Metall Mater 42:2291
[40] De Leon N, Yu X, Yu H, Weinberger C, Thompson G (2015) Bonding effects on the slip differences in the B1 monocarbides. Phys Rev Lett 114:165502
[41] Sciti D, Guicciardi S, Nygren M (2008) Densification and mechanical behavior of Hfc and Hfb2 fabricated by spark plasma sintering. J Am Ceram Soc 91(5):1433
[42] Song K, Xu Y, Zhao N, Zhong L, Shang Z, Shen L, Wang J (2016) Evaluation of fracture toughness of tantalum carbide ceramic layer: a vickers indentation method. J Mater Eng Perform 25(7):3057
[43] Ferro D, Rau JV, Albertini VR, Generosi A, Barinov SM (2008) Pulsed laser deposited Hard Tic, Zrc, Hfc and Tac films on titanium: hardness and an Energy-dispersive x-ray diffraction study. Surf Coat Technol 202(8):1455
[44] Zhang C, Gupta A, Seal S, Boesl B, Agarwal A (2017) Solid solution synthesis of tantalum carbide-hafnium carbide by spark plasma sintering. J Am. Ceram Soc 100(5):1853–1862